Turning black soldier fly rearing by-products into valuable materials: Valorisation through chitin and chitin nanocrystals production

Alexis Falgayrac, Virginie Pellerin, Cécile Terrol, Susana C M Fernandes

Carbohydrate Polymers 344 (2024) 122545

Contents lists available at ScienceDirect

Carbohydrate Polymers

journal homepage: www.elsevier.com/locate/carbpol

Turning black soldier fly rearing by-products into valuable materials: Valorisation through chitin and chitin nanocrystals production

Alexis Falgayrac [a,b,c], Virginie Pellerin [a], Cécile Terrol [c], Susana C.M. Fernandes [a,b,*]

[a] Universite de Pau et Pays de l'Adour, E2S UPPA, CNRS, IPREM UMR 5254, 64000 Pau, France
[b] MANTA – Marine Materials Research Group, Universite de Pau et des Pays de l'Adour, E2S UPPA, 64600 Anglet, France
[c] Agronutris, R&D Department, 31650 Saint-Orens de Gameville, France

ARTICLE INFO

Keywords:
Hermetia illucens
BSF
Nanochitin
Chitin
Circular economy
Insect industry
Side streams valorisation

ABSTRACT

The industry of insect-based proteins as feed and food products has been encountering a huge development since the last decade, and industrial-scale factories are now arising worldwide. Among all the species studied, Black Soldier Fly is one of the most promising and farmed. This rearing activity generates several by-products in the form of chitin-rich biomass that can be valorised to keep a virtuous production cycle embedded in the scope of the bioeconomy. Herein, we report the isolation of chitin and, for the first time, chitin nanocrystals (ChNCs) from all the BSF rearing by-products, i.e., moults (larval exuviae, puparium) and dead adults. Extraction yields, were dependent on the type of by-products and ranged from 5.8 % to 20.0 %, and the chemical structure of the extracts exhibited typical features of α-chitin, confirmed by FTIR, NMR, XRD and TGA analysis. Both STEM in SEM and AFM analysis confirmed the isolation of chitin nanocrystals presenting a rod-like morphology. The average nanocrystal height estimated by AFM ranged from 13 to 27 nm depending on the by-product sample. The following results highlighted the potential of BSF rearing by-products, promoting an approach to valorise those industrial waste and paving the way towards insect-based biorefinery.

1. Introduction

In the context of the growing world population, concerns are rising towards the food supply chain and the related impact on climate change. With global demand for agricultural products expected to increase by 15 % in the coming decade, scientists recommend reforming the food system to avoid an increase of its environmental footprint by 60–90 % between 2010 and 2050 (OECD, 2019); (Springmann et al., 2018). Considering the current situation, the search for alternative protein sources, in particular from insects, holds a central place in providing sustainable products worldwide. The production of insect-derived proteins shows environmental benefits compared to traditional livestock, consuming less land and water, leading to the emergence of a new industry based on the rearing of insects as food and feed ingredients (van Huis, 2013). In the last decade, numerous companies have emerged and insect-production plants are now arising everywhere on the globe.

Several insect species have been studied and implemented for their specific ability to bioconvert organic waste, such as manure, fruits or agriculture-wastes, into valuable proteins and lipids, thus, offering a solution for the management of food waste and loss (Ojha et al., 2020). Among them, the Black Soldier Fly (BSF, *Hermetia illucens*) has gained particular interest as a tangible source of alternative proteins and fats, having already found a market as feed ingredients for pet food, pigs, poultry and aquaculture fields. With growing volumes annually produced, companies are now facing the side streams generated by their activity (Chavez, 2021). Therefore, seeking solutions to valorise them in a circular model of development, with the opportunity to develop insect biorefineries is crucial. Throughout the BSF life cycle, different by-products can be found, mainly in the form of chitin-rich biomass, thus, providing a potential stable source of chitin and its derivatives (Nurfikari & de Boer, 2021). Insect exoskeleton is a composite structure where chitin acts as a matrix associated with proteins, lipids and minerals in specific cases (Muthukrishnan et al., 2022); (Jia et al., 2022).

Chitin is the second most abundant polysaccharide on Earth, with 10^{11} tons annually biosynthesized by living organisms as a structural component (Hahn et al., 2020). Chemically, it's a linear copolymer of randomly distributed *N*-acetylglucosamine as major unit and N-glucosamine as minor one, linked by β,1 → 4 glycosidic bond. It exhibits three allomorphic crystal structures, α, β and γ, following the parallel or antiparallel polymer chain arrangement (Arnold et al., 2020). Depending on

* Corresponding author at: Universite de Pau et Pays de l'Adour, E2S UPPA, CNRS, IPREM UMR 5254, 64000 Pau, France.
E-mail address: susana.fernandes@univ-pau.fr (S.C.M. Fernandes).

https://doi.org/10.1016/j.carbpol.2024.122545
Received 15 April 2024; Received in revised form 24 June 2024; Accepted 23 July 2024
Available online 25 July 2024

the source from which it is extracted, chitin's intrinsic physico-chemical features might slightly differ (Kaya et al., 2017). However, its overall functional properties such as biodegradability, non-toxicity and biocompatibility offer this natural polymer a wide range of applications in economically important sectors, including biomedicine, cosmetics or agriculture among others (Tamura et al., 2011); (Lv et al., 2023); (Sharp, 2013); (Olza et al., 2023); (Fernández-Marín et al., 2022); (Fernández-Marín et al., 2021); (Zubillaga et al., 2020); (Zubillaga et al., 2018);

One interesting aspect is the ability to derive chitin into its nanometric form, nanochitin, thus offering enhanced characteristics, like high mechanical properties, high surface area, low density and reactive surface groups (Kishida et al., 2022); (Salaberria et al., 2015). For example, nanochitin can be used as a reinforcing agent in films to produce nanocomposites or as stabilising agents in Pickering emulsions systems (Salaberria et al., 2017); (Fernández-Marín et al., 2020); (Jiménez-Saelices et al., 2020). Generally, nanochitin is obtained by top-down methods disintegrating chitin bundles via controlled chemical or mechanical reaction and can be classified whether it displays fibre- or rod-like structure, namely chitin nanofibers (ChNFs) and chitin nanocrystals (ChNCs) (Bai et al., 2022).

Recently, the growing interest towards the insect industry has shed light upon insect-chitin and more specifically black soldier fly-derived chitin, with an increased number of studies on its extraction, intrinsic properties, potential applications, and lately nanochitin production (Złotko et al., 2021); (Khatami et al., 2024); (Triunfo et al., 2022); (Xiong et al., 2023); (Rampure et al., 2023); (Lee et al., 2022); (Mannucci et al., 2024); (Feng et al., 2023); (Pasquier et al., 2021). Nevertheless, most research has focused on the production of chitin nanofibers (ChNFs). Furthermore, these ChNFs have been extracted from larvae or prepupae which are the main products of interest of insect-based proteins activity (Pasquier et al., 2021); (Le et al., 2023), and not from BSF rearing wastes generated by this industry (larval exuviae, puparium and dead adult flies).

With the determination to close the loop and develop a circular production model, we are convinced that the valorisation of all the chitinous side streams of the BSF rearing would be beneficial to this industry. Instead of using this waste in methanization or rendering processes as a final treatment step, the idea is to transform it into new products/materials with high economic added value and approaching the zero-waste system.

Therefore, the aim of this work is to extract, characterize and compare the yield, physico-chemical and morphological properties of chitins and chitin nanocrystals (ChNCs) isolated from BSF by-products generated by the industry of insect-based proteins: i.e., larval exuviae, puparium and dead imago (dead adult fly). To the best of our knowledge, the isolation of chitin nanocrystals (ChNCs) from all the BSF rearing by-products is investigated for the first time in this study. Thus, herein, a conventional chemical extraction is used in order to compare the properties of the chitins and ChNCs obtained with those in the literature and with a commercial chitin derived from crustaceans. This could help to assess the potential of this recent biomass as feedstocks for natural functional polymers with the long-term target of an insect biorefinery implementation.

2. Materials and methods

2.1. Chemicals and raw materials

The by-products generated by black soldier fly-rearing activities, i.e., the larval exuviae, the puparium and the dead imago, were kindly supplied by Agronutris (France) between 2023 and 2024. HCl (37 %, ACS reagent) and anhydrous NaOH pellets were purchased from Merck, diethyl ether ($\geq$ 99.7, ACS reagent) was obtained from VWR, and NaOCl aqueous solution (12–15 % available chlorine) acquired from Abcr GmbH. All reagents were used as received without further purification. Commercial α-chitin (presenting a Degree of Acetylation (DA) of 94.8 % and a Crystallinity Index (CI) of 77 %, characterized *in-house*) derived from shrimp shells was provided by Mahtani Chitosan Pvt. Ltd. (India) and used as reference chitin material.

2.2. Biomass harvesting and homogenisation

Three types of resources produced as rearing wastes during the life cycle of *H. illucens* were considered as potential alternative chitin sources: (i) the larval exuviae – larval moult; (ii) the puparium – pupal shell left after fly emergence, and (iii) the dead imago – dead fly. First, the BSF larvae were grown on a semi-industrial substrate composed of discarded grains, wheat soluble, and co-products arising from beetroot and potato processing. Then, the larval exuviae (BSFE) samples were manually collected and separated from the breeding substrate at the last larval stage, while the puparium (BSFP) samples were harvested in the emergence rack, and the dead imago (BSFI) samples were collected from the fly aviaries at the end of their life cycle. Each resource was washed extensively with tap water to remove impurities, sieved and dried at 60 °C until stable mass. Homogenisation was done by grinding the whole insect sample into a fine powder using a Retsch GM200 laboratory knife mill. The samples were kept in a hermetic storage container and stored at −21 °C until further use.

2.3. Proximate analysis of raw samples

The proximate analysis of by-products was performed to investigate the initial composition of each sample before their valorisation. Moisture and ash content were determined gravimetrically by drying samples in an oven, respectively, at 103 °C for 4 h and at 600 °C until no carbonaceous particles was left, leading to the obtention of whitish or reddish ash. Soxhlet extraction was used to calculate the crude oil content using diethyl ether as solvent. The nitrogen amount within samples was obtained with the Dumas Method, and a nitrogen-to-protein conversion factor of 6.25 was applied to calculate the protein content (Miller et al., 2007).

2.4. Extraction of chitin from black soldier fly (BSF) by-products

Chitin was extracted from the three by-products using conventional chitin extraction method adapted to insect source proposed by (Hahn et al., 2021), with slight modifications. The process involved the realisation of 4 extraction steps to recover the remaining chitin as the insoluble residue. Delipidation was first carried out using a Soxhlet apparatus with diethyl ether to solubilize and remove apolar compounds, which may hinder interactions with chemical reagents because of hydrophobic repulsions (Nurfikari & de Boer, 2021). Approximately 5 g of initial biomass were loaded in the cellulose thimble and the Soxhlet system was run for 5 h allowing 20–24 cycles depending of the by-product. The degreased powder was air-dried overnight under a fume hood. The samples were therefore demineralised with a 1 M HCl solution (solid:liquid ratio of 1:20) for 1 h at 100 °C. The mixture was filtered, washed extensively to reach a neutral pH and oven-dried overnight at 60 °C. The deproteination was achieved by treating the demineralised sample with a solution of 2 M NaOH (solid:liquid ratio of 1:30) for 4 h at 90 °C. The powder was recovered by filtration, washed and dried overnight at 60 °C. Finally, the bleaching of the sample was performed to remove residual pigments with a 6 % NaOCl aqueous solution (solid:liquid ratio of 1:40) for 1 h at 60 °C. After filtration, the chitin samples were washed with water to remove solvent from the powder and dried overnight at 60 °C in a circulating oven until stable mass.

2.5. Isolation of nanocrystals from black soldier fly chitin

Acid hydrolysis with concentrated hydrochloric acid was performed to isolate the crystalline phase of the chitin polymer by removing the amorphous part from the material. The process used, was adapted from

the method described in previous work (Salaberria et al., 2014). An amount of 400 mg of the extracted chitin from each type of by-product was incubated in a reactor with 3 M HCl at 100 °C for 90 min at a solid: liquid ratio of 1:30. The reaction was quenched afterwards, by cooling the mixture with an ice bath and adding a 5-fold volume of distilled water. The nanocrystal suspensions were left to sedimentation, and the supernatant was discarded to recover a blurry suspension. The nanocrystal suspensions were washed by two centrifugation cycles (5927 *g*, 5 min at 5 °C) to remove excess acid before being transferred to a dialysis membrane (SpectraPor 3.5 kDa MWCO regenerated cellulose membrane from Spectrum Laboratories). Dialyses were done overnight in large volumes of distilled water to reach a neutral pH. The nanocrystal suspensions were then concentrated and recovered by centrifugation (27,216 *g*, 20 min at 5 °C). One fraction, per each concentrated suspension, was reserved in the wet form to analyse the morphological and colloidal properties and the other fraction was freeze-dried to obtain powdered chitin nanocrystal samples for the other analyses. The wet nanocrystals fractions were furthermore sonicated and homogenised to allow their morphological characterization (see Sections 2.7.6, 2.7.7 and 2.7.8).

2.6. Determination of the chitin (Ch) extraction and nanocrystals isolation (ChNC) yield

The chitin extraction and chitin nanocrystals yield for each by-product were determined by gravimetry, using the Eqs. (1) and (2), respectively:

$$Chitin\ Yield\ (\%) = \frac{m_{Ch}}{m_{raw}} \times 1000 \quad (1)$$

where m_{Ch} is the mass of the dried powdered samples obtained after the bleaching treatment, corresponding to the chitin residue, and m_{raw} is attributed to the initial dry mass of the by-product involved in the purification process.

$$Chitin\ nanocrystals\ Yield\ (\%) = \frac{m_{ChNC}}{m_{Ch}} \times 1000 \quad (2)$$

where m_{ChNC} is the mass of the freeze-dried chitin nanocrystals, and m_{Ch} is attributed to the initial dry mass of chitin involved in the acid hydrolysis process.

2.7. Physico-chemical characterization of the raw materials, chitin and chitin nanocrystals

2.7.1. Fourier transform infrared spectroscopy (FTIR)

The Attenuated Total Reflectance-FTIR (ATR-FTIR) spectra of the raw by-products, ether extracts, extracted chitin, commercial α-chitin, and obtained powder chitin nanocrystals were analysed in terms of their chemical structure by using a Nicolet iS50 FTIR spectrometer (Thermo Fisher Scientific, USA). The spectra were recorded from a range of 4000–400 cm^{-1}, with a resolution of 4 cm^{-1} and an accumulation of 64 scans.

2.7.2. Solid state ^{13}C-nuclear magnetic resonance spectroscopy (^{13}C ss-NMR)

The solid-state ^{13}C cross-polarized magic-angle spinning nuclear magnetic resonance (^{13}C CP-MAS NMR) experiments were performed to assess the purity of the chitin and chitin nanocrystal samples obtained from the insect by-products. The spectra were recorded on a Bruker Avance III 500 MHz spectrometer (Bruker, USA), using a 4 mm CP-MAS probe, with a sample spinning rate of 11 kHz and a contact time of 2 s. The degree of acetylation (DA%) of each sample was calculated from the ratio of the integral of the methyl carbon over the integrals of the polysaccharide ring using Eq. (3) (Kasaai, 2010):

$$DA(\%) = \frac{I_{CH_3}}{(I_{C1} + I_{C2} + I_{C3} + I_{C4} + I_{C5} + I_{C6}) \times \frac{1}{6}} \times 100 \quad (3)$$

2.7.3. X-ray diffraction (XRD)

The X-ray diffraction pattern of the extracted chitin and isolated chitin nanocrystals was obtained with a diffractometer (Rigaku, Tokyo, Japan) operating at 40 kV and 40 mA to determine the crystalline features of the analysed samples. A FR-X rotating anode Cu-kα anode (λ = 1.54060 Å) was used as the radiation source and the angular range was set between 5° and 40° in 2Θ with a 3-circle partial chi goniometer.

2.7.4. Scanning electron microscopy (SEM)

The morphology of the raw by-products and chitin samples was investigated via a Hitachi SH-3000 scanning electron microscope (Hirox Europe, Limonest, France), operating at an acceleration voltage of 25 kV. The powdered samples were first sputter-coated with gold plasma under vacuum using a Denton Vacuum Desk V sputter coater (Moorestown, NJ, USA) with a current of 30 mA for 60 s.

2.7.5. Scanning transmission electron microscopy in scanning electron microscopy (STEM in SEM)

Scanning transmission electron microscopy in Scanning Electron Microscopy (STEM in SEM) was used to analyse the morphological features of the isolated chitin nanocrystals with a Thermo Scientific Apreo 2 scanning electron microscope (Thermo Fischer Scientific, Waltham, USA), operating at an acceleration voltage of 30 kV with a STEM detector. Before the analysis, wet chitin nanocrystals derived from each by-product were dispersed in ultrapure water to obtain a diluted suspension of nanocrystals (0.01 $g.L^{-1}$). The mixture was then subject to an ultrasonication treatment with a 500 W Sonics Vibracell probe set at a 30 % amplitude for 10 min. A 2 μL droplet of the sonicated suspension was deposited on a 200 mesh Cu TEM grid (Ted Pella Inc. type B) and excess water was removed carefully from the grid with a paper before insertion in the STEM chamber to proceed to the morphological investigations.

2.7.6. Atomic force microscopy (AFM)

Atomic force microscopy was performed to assess the nanocrystal's morphology and size, operating using a MultiMode 8 AFM (Bruker, USA). The images were taken in PeakForce Quantitative Nano-Mechanical mode under ambient conditions using ScanAsyst probe (0.4 nN) at 2 kHz. Before the analysis, wet chitin nanocrystals derived from each by-product were dispersed in ultrapure water to obtain a diluted suspension of nanocrystals (0.003 $g.L^{-1}$). The mixture was then subject to an ultrasonication treatment with a 500 W Sonics Vibracell probe set at a 30 % amplitude for 20 min, in addition to a 5 min treatment with a Unidrive X1000D homogenizer operating at 10000 rpm. 2 μL of the sonicated suspension was deposited on an ozone cleaned silica wafer and air-dried overnight under a fume hood. The average height of the nanocrystal's suspension was estimated with the NanoScope Analysis software, with a sample size of 50 nanocrystals.

2.7.7. Thermogravimetric analysis (TGA)

Thermogravimetric investigations were carried out using a TGA 2 Mettler Toledo thermogravimeter (Mettler Toledo, USA). Approximately 2–10 mg of grounded by-products, extracted chitin and chitin nanocrystal samples were weighted in an alumina crucible and heated from 30 to 900 °C with a heating rate of 20 °C min^{-1}, and a gas flow rate of 50 mL min^{-1} in both nitrogen and air atmosphere. The samples were stored at room temperature before analysis and were not dried in an oven beforehand, thus, retaining their residual humidity.

2.7.8. Zeta potential and dynamic ligh scattering (DLS)

The colloidal properties of the produced nanocrystals were evaluated by measuring the zeta potential of chitin nanocrystal suspensions from

each source (0.005 g.L^{-1}), with a Malvern Zetasizer Nano ZS (UK) coupled with an MPT-2 autotitrator system. Ultrasonication of the suspensions was performed before the analysis with a 500 W Sonics Vibracell probe set at a 30 % amplitude for 20 min, in addition to a 5 min treatment with a Unidrive X1000D homogenizer operating at 10000 rpm. A folded capillary zeta cell was employed and the diluted suspensions in ultrapure water were investigated on a pH range going from 2 to 12, adjusted with 1 M NaOH and 1 M HCl buffer solutions. Dynamic light scattering was also used to estimated *Z*-average diameter in the same conditions with the Zetasizer Nano ZS (UK).

3. Results and discussion

3.1. Chemical composition of the raw by-products

Understanding the composition of the initial material is of vital importance in the scope of waste valorisation through extraction procedure. In this sense, the proximate analysis is a valuable tool to obtain insights from the elements that constitute a biological material. The composition of each raw by-product investigated is reported in Table 1.

Moisture content was measured as 18.0 %, 11.1 % and 40.5 % for BSFE, BSFP, and BSFI while their ash content accounted for 5.1 %, 23.3 % and 3.2 %, respectively. Even though mineral is often found in only a low proportion in insects compared to crustaceans (Kamal et al., 2020); (Hahn et al., 2020), it is noteworthy that the studied by-products show inorganic material, in particular BSFP, exhibiting a particularly high concentration of minerals, where it could act as a protective layer against external stresses, as recently demonstrated by Rebora et al. (2023). The same observations were made looking at the thermogravimetric analysis (TGA) profiles of the raw samples under oxidizing oxygen atmosphere and their remaining residues at 900 °C, where it is assumed that only inorganic material may be present (Supplementary Fig. S1c and Supplementary Table S1).

With values comprised between 2 and 4 %, fat content was found to be relatively low in larval exuviae and puparium moults, compared to adult BSF exhibiting a crude oil content of almost 25 %. Those results are in accordance with previous studies done by Triunfo et al. (2022) and can be explained by the fact that insects store energy in the form of fat in their body such as BSF adult specimens, while moulted exoskeletons are expected to display only structural lipidic compounds composing the different layer of the cuticle (Arrese & Soulages, 2010); (Bhavsar et al., 2021). Although the general appearance of the crude oils obtained from the BSF by-products differs (see Supplementary Fig. S2), their chemical composition was comparable based on ATR-FTIR analysis with characteristic bands attributed to aliphatic compounds around 2900 cm^{-1} and carbonyl esters at 1710 cm^{-1} (see Supplementary Fig. S1b).

As expected, each raw by-product contains an important proportion of proteins ranging from 26 % up to 48 %. The type of proteins encountered in BSF by-products are assumed to be mainly cuticular proteins, especially for the moults, larval exuviae and puparium. Those are insoluble structural proteins, which can be tightly bound to catecholamine compounds and chitin presumably by cross-links, during the sclerotization process where the insect cuticle hardened and darkened (Peter et al., 1984). This reaction is also accompanied by the deposition of granular melanin, giving the black colour encountered in the cuticle (Andersen, 2010).

Knowing the following composition of the raw by-products and how biomolecules are assembled within the matrix of the biological material may better guide suitable design and efficiency of chitin extraction approaches. Hence, the deproteinisation should represent a key step to obtain purified chitin, in particular for the purification of sclerotized samples (i.e. the puparium). Herein, considering the rather high content of minerals for the considered BSF resources and more particularly the puparium, minerals removal should not be overlooked to reach a better extraction for the present samples, in contrast to other studies with different insect species where demineralisation was not needed (Kamal et al., 2020); (Khatami et al., 2024).

Table 1
Proximate composition of the by-products derived from black soldier fly-rearing activity.

Analysed parameters	BSFE	BSFP	BSFI
Moisture content (%)	18.0	11.1 ± 0.6[b]	20.6 ± 0.6[b]
Crude ash (%)	5.1	23.3 ± 0.9[b]	3.2 ± 0.2[b]
Crude oil (%)	2.4 ± 0.2[a]	3.9 ± 0.8[a]	24.7 ± 0.5[a]
Protein content (%)	25.7	44.3 ± 1.3[b]	48.1 ± 1.4[b]

[a] Values are presented as mean ± standard deviation ($n = 3$).
[b] Values are presented as single results ± uncertainty.

3.2. Physico-chemical properties of the extracted chitin

The extraction of chitin from the BSF rearing by-products was conducted following a four-step chemical approach, and the ensuing products were obtained in the form of powder or flakes presenting a brownish or whitish colour (see Supplementary Fig. S2). Chitin yields of 16.2 %, 20.0 % and 5.8 % were found for larval exuviae, puparium and dead adult fly, respectively (Table 2), highlighting the potential of the exuviae, puparium, as alternative chitin sources. Brigode et al. reported similar values for the chitin content in dead adult fly and puparium, with 7.7 % and 25.4 % (Brigode et al., 2020). Valorisation of chitin from larval exuviae is less described in the literature, however Soetemans et al. outlined an extraction yield of 31.1 % from larval sheddings (Soetemans et al., 2020). The chitin content obtained in the present study was lower, which may be related with the composition of the initial by-products that is particularly influenced by the variations in the rearing conditions (e.g. feeding substrate) impacting the larval stages. To obtain further insights into the physico-chemical features of the extracts and assess their purity, as well as their composition, several characterization techniques were performed.

Solid-state ^{13}C NMR spectra of the obtained chitin from the BSF by-products are presented in Fig. 1a. Characteristic resonance peaks of chitin could be identified for each sample with some variations regarding purity and composition (see Supplementary Table S2). All samples, dead imago (BSFI-Ch), puparium (BSFP-Ch) and larval exuviae (BSFE-Ch) showed similar chemical structure, with signals between 58.2 and 101.4 ppm attributed to the carbon atoms of the glucopyranosyl ring, labelled from C1 to C6 (Fig. 1a). The peak of the methyl group (CH_3) was found at 20.1 ppm while the one of the carbonyl groups (C=O) was located around 170.8 ppm. The presence of a split into

Table 2
Yields of chitin extraction and chitin nanocrystal isolation, Degree of Acetylation (DA), and maximal degradation temperature under air and nitrogen atmosphere of the extracted chitin (Ch) and isolated chitin nanocrystals (ChNC) from BSF by-products.

Sample	Yield Ch (%)	Yield ChNC (%)	DA (%)	Td_{max} under Air atmosphere (°C)	Td_{max} under N2 atmosphere (°C)
BSFE-Ch	16.19 ± 0.31	–	≈ 57	334.07 ± 4.01	376.54 ± 2.68
BSFP-Ch	19.98 ± 1.39	–	97	333.19 ± 2.47	395.17 ± 0.94
BSFI-Ch	5.84 ± 0.13	–	100	340.01 ± 2.48	395.79 ± 0.43
BSFE-ChNC	–	69.40	≈ 61–66	332.10 ± 0.36	360.46 ± 0.68
BSFP-ChNC	–	70.93	96	338.76 ± 0.53	397.59 ± 0.55
BSFI-ChNC	–	74.76	100	339.70 ± 1.34	392.85 ± 0.12

Yields of chitin extraction and degradation temperature values are presented as mean ± standard deviation.

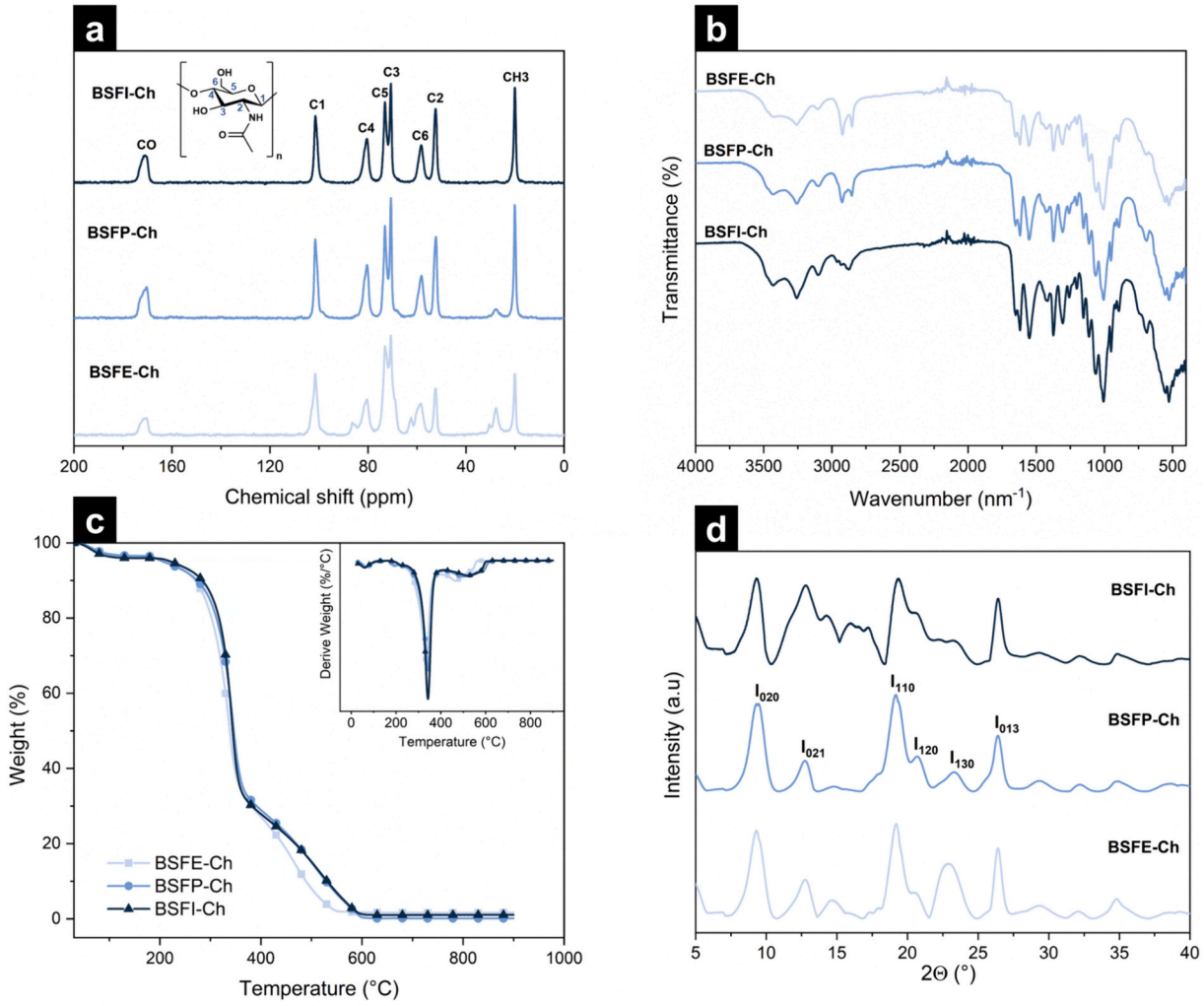

Fig. 1. ^{13}C NMR spectra (a), FTIR spectra (b), TGA and DTG profile under air atmosphere (c), and XRD diffractograms (d) of the chitins obtained from BSF imago (BSFI-Ch), BSF larval exuviae (BSFE-Ch) and BSF puparium (BSFP-ch).

doublet for C5 and C3 peaks at 73.0 and 75.6 ppm, indicate that the following chitins are assimilable to the α-chitin polymorph. Nonetheless, BSFP-Ch and BSFE-Ch NMR spectra displayed additional peaks. BSFP-Ch revealed a small peak around 27.7 ppm which suggests the presence of residual proteins and/or catechols arising from the high degree of sclerotization in this type of exoskeleton moult (Kramer et al., 1995); (Hahn et al., 2021). In the case of BSFE-Ch, apart the characteristic chitin peaks, NMR spectrum showed an important peak at 27.7 ppm indicating the presence of remaining proteins, and resonance peaks at 62.4 and 86.3 ppm, suggesting the presence of cellulosic compounds. Pasquier et al. reported similar observations with chitin extracted from yellow mealworm containing up to 44 wt% of cellulose in the sample and presenting analogue peaks in ss-NMR analysis (Pasquier et al., 2021). This cellulose content may arise from particles of the rearing substrate which are still blended with the larval exuviae during the homogenisation treatment.

The degree of acetylation (DA) of all samples was determined by NMR analysis (Table 2). Chitins derived from dead imago and puparium were found to be highly acetylated (100 and 97 %, respectively), while the estimation of the DA value of larval exuviae is difficult to determine because of the presumed cellulose content.

ATR-FTIR spectra of the obtained chitin samples were assessed and compared with chitin extracted from shrimp (see Supplementary Fig. S3a). As observed in Fig. 1b, the three spectra displayed typical vibrational bands of chitin (see Supplementary Table 3) and similar to shrimp chitin. The absorption bands found in the region of 3430 and 3100 cm^{-1} were assigned to O—H and N—H stretching respectively, which are distinctive of the intermolecular hydrogen bond network. The amide II and III bands, visible at 1552 and 1308 cm^{-1}, were identified, as well as, a characteristic amide I band of the α-chitin form with a split into doublet at 1652 and 1620 cm^{-1}. A low-intensity shoulder was discerned around 1726 cm^{-1}, for BSFE-Ch and BSFP-Ch, confirming the presence of residual proteins as demonstrated before by NMR analysis. These two samples demonstrated also a unique pattern for the vibrational bands at 2922 and 2851 cm^{-1}, which was outlined for most of the FTIR spectra of chitin derived from insect cuticles (Brigode et al., 2020); (Soetemans et al., 2020); (Kaya & Baran, 2015); (H. Wang et al., 2020). Although the presence of these specific bands has been rarely described, recent research pointed out that it could result from organic impurities, possibly lipids considering the intensity of the CH_2 and CH_3 stretching bands, that exhibit a strong resistance to the purification treatment (Elkadaoui et al., 2024).

The thermogravimetric analysis (TGA) was performed under nitrogen and air atmospheres, allowing access to different information on the thermal behaviour of the samples. Nitrogen atmosphere as an inert environment, gives insights into the main organic degradation pattern of chitin, while air allows to explore the complete degradation of organic matter, allowing to quantify also the total inorganic matter content. Under the air atmosphere, as showed in Fig. 1c and Table 2, TGA and DTG profiles of BSF chitin displayed similar degradation stages

compared to shrimp chitin (see Supplementary Fig. S3c) with three visible weight losses and a distinct maximal degradation temperature. The first weight loss was assigned to the evaporation of residual water content in chitin. This occurrence was measured around 30 °C and 140 °C under air atmosphere, with a weight loss comprised between 3.4 and 4 % depending on the BSF sample. Then, the second and main degradation step was noted by a sharp degradation peak with a weight loss of about 70 % at 340 °C (Td_{max}), showing similar behaviour to shrimp chitin (63 % loss at 329 °C). This weight loss corresponds to the decomposition of the chitin polymeric structure, manifested by depolymerisation of the polysaccharide, ring dehydration and deterioration of acetylated and deacetylated units. A third degradation stage, specific to the air oxidizing atmosphere, reached a maximum of around 500–550 °C, with a weight loss of approximately 25 % for BSF samples and 27 % for shrimp-chitin. This was assigned to a combustion reaction of the carbonised chitin, alongside with a devolatilization of char. This data is in agreement with a previous study which investigated the degradation profile under air atmosphere of α-chitin obtained from *Polybius Henslowii* crab (McReynolds et al., 2022). The final residues at 900 °C were respectively, 1.27 %, 0.13 %, 1.09 % for BSFE-Ch, BSFP-Ch, BSFI-Ch and 2.3 % for Shrimp-ch. In agreement with FTIR and NMR analysis, these results confirmed that no inorganic impurities were left in the chitins after extraction. Under nitrogen atmosphere (see Supplementary Fig. 4a), and according to literature for α-chitin, all the samples exhibited two decomposition stages with the first one corresponding to water evaporation, and a second degradation step corresponding to sugar deterioration (H. Wang et al., 2020). However, BSFE-Ch sample showed a broader degradation peak, indicating the presence of impurities such as residual cellulosic compounds, and protein's traces (small degradation peak around 460 °C on the DTG profiles) (Zozo et al., 2022). All these observations were consistent with FTIR and NMR analysis. Residues at 900 °C for all the BSF-Ch and shrimp-Ch under an inert atmosphere ranged from 14 to 19 %, being higher than the ones under an oxidizing atmosphere and representing mainly chitin carbonised matter (biochar) knowing that few amounts of biominerals are found in the samples. The maximal degradation temperatures were 376 °C, 395 °C and 396 °C for chitin derived from larval exuviae, puparium and dead imago, respectively, while chitin derived from shrimp was of 383 °C. The following results were in accord with Td_{max} values under N2 atmosphere for α-chitin (350–400 °C) (Paulino et al., 2006).

XRD diffraction profiles of the extracted BSF chitins are presented in Fig. 1d. Six main diffraction peaks were observed for all the samples, corresponding to the crystal planes of α-chitin at 2Θ values of 9.3° (020), 12.8° (021), 19.2° (110), 20.6° (120), 23.3° (130), 26.4° (013), being consistent with the literature (Ngasotter et al., 2023); (Salaberria et al., 2014). Accordingly with the NMR and TGA results, the broader peak at 22.9° for BSFE-Ch sample could be attributed to a partial contribution of cellulosic content with cellulose Iα (110) plane overlapping with the α-chitin (130) plane (Pasquier et al., 2021). XRD data values for each sample are depicted in Supplementary Table S4. For all diffractograms, highest intensity peak was recorded for (110) and BSFP-Ch showed a sharpest and more defined peak, suggesting a higher crystallinity.

The surface morphology of the powdered chitin samples (Fig. 2) was assessed and compared to the powdered raw by-products (Fig. S5). When considering, biological material such as insect cuticle, morphological features play an essential role regarding chitin's functionality and usage. Previous studies have shown that chitin surface morphology differs depending on the species, the gender and the growth stage, with four distinct morphology types depending on the presence or absence of pores and fibrillar structure (Kaya et al., 2015). BSFI-Ch (Fig. 2a) displayed the most diverse surface morphology with microporous surface and hexagonal arrangement as well, depending on the body part considered, which can be linked to the different functions needed to operate for the adult stage. Here, chitin's role as a scaffold can be clearly highlighted, with similar structures found for the raw by-products, although, being less dense and logically not decorated with other organic and inorganic compounds (see Supplementary Fig. S5). In Fig. 2b and c, the morphology of BSF chitin derived from spent shells is presented with a unique honeycomb-like pattern composed of hexagonal/pentagonal tiles and a dense surface. Although not visible on those

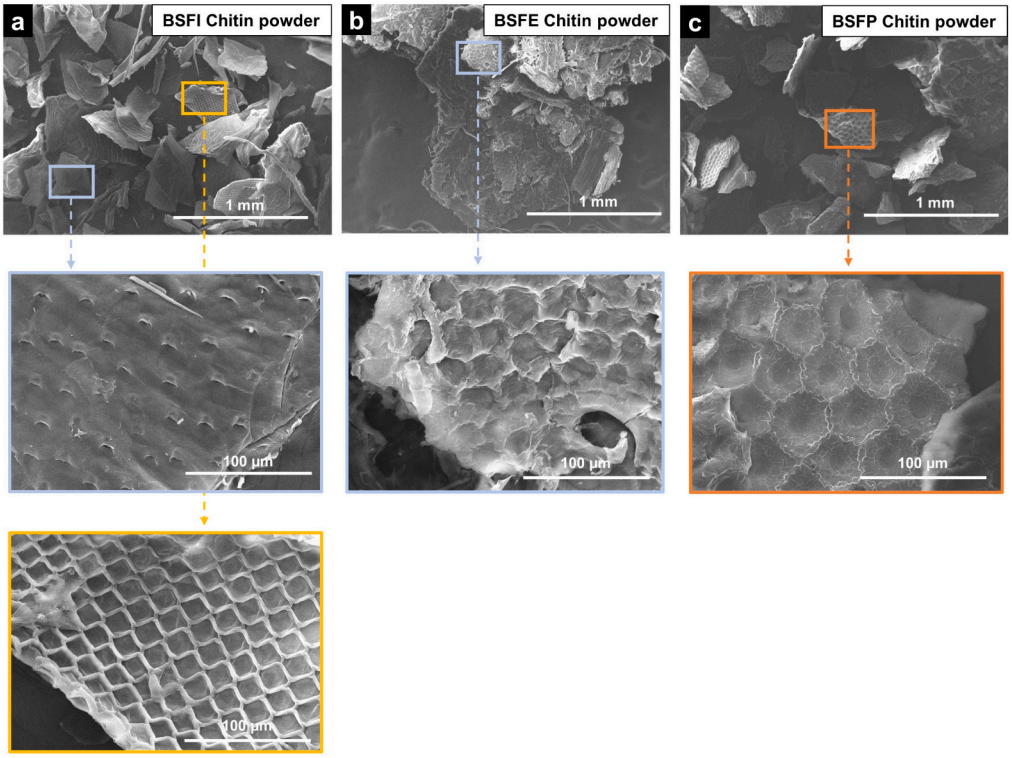

Fig. 2. SEM images (magnification ×50 and ×500) of chitin powder extracted from dead imago (a), larval exuviae (b), and puparium (c).

micrographs some porous and/or fibrillar structures at the nanometric scale can be assumed based on previous studies (Purkayastha & Sarkar, 2020); (Triunfo et al., 2022).

The physico-chemical characterization of the chitin extracted from BSF-rearing by-products allowed to assess their properties and purity, which are important data to evaluate the scope of coming applications and the approach to produce its main derivatives: chitosan and/or nanochitins. Here, the chitin from dead imago (BSFI) showed the best purity with characteristics close to the one derived from shrimp, despite displaying a low yield (see Table 2). Some impurity traces were found in larval exuviae (cellulose and proteins) and puparium (proteins), confirmed by FTIR, NMR and TGA analysis. This may arise, for the latest resource, from the high degree of sclerotization of proteins. Therefore, modifications to the extraction process could be beneficial, given that BSFP-chitin represents a promising chitin source with an initial biomass extraction yield reaching almost 20 %, and being among the three by-products, the most generated.

3.3. Analysis of the obtained BSF chitin nanocrystals (ChNCs)

After chitin extraction from BSF rearing by-products (i.e. larval exuviae, puparium and dead imago), the derivatisation into chitin nanocrystals (ChNC) was undertaken by conventional acid hydrolysis. During this process, amorphous regions with low lateral order are hydrolysed and dissolved while the crystalline part more resistant to acid attacks remains, emerging as rod-like particles (Scheme. 1). The isolated chitin nanocrystals present gel-like forms with whitish colour (see Supplementary Fig. S2). Chitin nanocrystals yields ranged between 70 and 75 %, being similar with those reported in literature for shrimp-derived nanocrystals (Narkevicius et al., 2019).

3.3.1. Physico-chemical properties of chitin nanocrystals

The physico-chemical properties of the ensuing chitin nanocrystals were investigated in the same regard as for chitin allowing to identify potential changes in features after the ChNC isolation process. NMR, FTIR and TGA analysis of the chitin nanocrystals are presented in Fig. 3. Overall physico-chemical parameters of the resulting nano-objects were comparable to their chitin analogues with slight differences.

^{13}C NMR spectra of chitin nanocrystals isolated from larval exuviae, puparium and dead imago, respectively labelled as BSFE-ChNC, BSFP-ChNC and BSFI-ChNC, showed similar spectra than BSF chitins (Fig. 3a). All the spectra displayed characteristics resonance peaks of α-chitin molecule with sugar ring carbon atoms (C1–C6), methyl (CH3) and carbonyl (C=O) peaks being located in the same range than the correlated chitins (see Supplementary Table S5). The same impurities (cellulosic compounds) and residual protein trace signals were found only for larval exuviae chitin nanocrystals samples. The DA was of 96 %, 100 % and 61–66 %, respectively for BSFP-ChNC, BSFI-ChNC and BSFE-ChNC (Table 2). As for BSFE-Ch, the DA determination of BSFE-Ch was affected by the probable cellulosic content.

FTIR spectra of ChNCs (Fig. 3b) showed a comparable pattern to extracted BSF chitins, with vibrational bands identified at, 1619–1654 cm^{-1} (Amide *I*), 1552 cm^{-1} (Amide II), 1307 cm^{-1} (Amide III) and 1154 cm^{-1} (saccharide ring), typical from chitin chemical structure (see Supplementary Table S6). Interestingly, the bands ascribed to potential lipids and residual proteins around 2900 cm^{-1} and 1710 cm^{-1}, respectively, were not identified, indicating a further purification during the isolation process regarding the proteins and lipids content. In this sense, FTIR spectra of chitin nanocrystals from BSF-rearing by-products displayed identical features to ChNCs extracted *in-house* from shrimp chitin (see Supplementary Fig. S6a).

Thermogravimetric analysis curves under air atmosphere of BSF ChNCs are presented in Fig. 3c and their TGA and DTG profiles under an inert atmosphere are depicted in Supplementary Fig. S4b. The thermal behaviour of the ensuing BSF ChNCs revealed similar trends, either under air or nitrogen atmosphere, when compared to extracted BSF chitins. Under an oxidizing atmosphere, the three degradation stages corresponding to water evaporation, chitin degradation and biochar devolatilization were observed at similar temperatures. Almost no residues were left at 900 °C, meaning that no mineral content was found within the samples. In the inert environment, BSF-ChNCs presented the same degradation profile as BSF-chitin, with at least two distinct weight losses for all nanocrystal samples. The same additional degradation stage for protein traces was present around 458 °C for BSFP-ChNC and BSFE-ChNC. For the latest, the degradation peak at Td_{max} appeared more defined and sharper than BSFE-Ch, despite being still affected to some extent by impurities (e.g. cellulose content). The Td_{max} as well as the main reviewed physico-chemical parameters of BSF ChNCs are summarized in Table 2.

Chitin nanocrystals diffractograms are shown in Fig. 3d and the major diffraction peaks' position with their respective attribution are given in Supplementary Table S7. Similarly, as NMR results for the nanocrystals, ChNCs crystalline features derived from BSF by-products were similar to the chitin extracts starring a typical pattern of α-chitin. A better definition of all the crystalline peaks and more particularly the one corresponding to (110) plane, was noticed for each sample, indicating an increase in the overall crystalline behaviour compared to BSF chitins.

3.3.2. Morphological properties of the BSF-ChNC

Morphological features of the isolated BSF chitin nanocrystals were observed by combining STEM in SEM and AFM analysis, and, as displayed in Fig. 4 all samples showed a rod-like morphology. Based on STEM in SEM images, BSFI-ChNC samples showed smaller rod-like nano-objects in width and length comparing with BSFP-ChNC and BSFE-ChNC samples. Nevertheless, Fig. 4c and e, corresponding to puparium and larval exuviae ChNC samples, appear to have higher level of aggregation that may be due to the presence of some residual proteins and cellulosic complexes demonstrated by NMR and TGA.

STEM in SEM micrographs of BSF-ChNC were compared to *in house* isolated chitin nanocrystals from commercial shrimp chitin (see Supplementary Fig. S6b) and TEM images of diluted suspension of shrimp-derived nanocrystals from literature, which presented a typical morphology of rod-like particle with high aspect ratio (Gopalan Nair et al., 2003). Interestingly, the isolated BSF-ChNCs revealed similar rod-like morphology but with longer lengths and thinner widths.

AFM images in peak force mode of the diluted BSF nanochitin suspensions, also displayed nanometric chitin particles in the form of whiskers. The average heights measured from the AFM images, showed values ranging from 13 to 27 nm depending on the samples (Table 3 and Supplementary Fig. S7). The lower height (13 nm) was ascribed to BSFI-ChNC, being consistent with STEM in SEM observations.

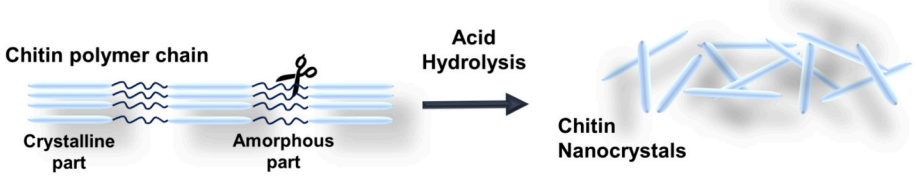

Scheme 1. Schematic representation of the chitin nanocrystal isolation from chitin polymer chain by acid hydrolysis process (Narkevicius et al., 2019).

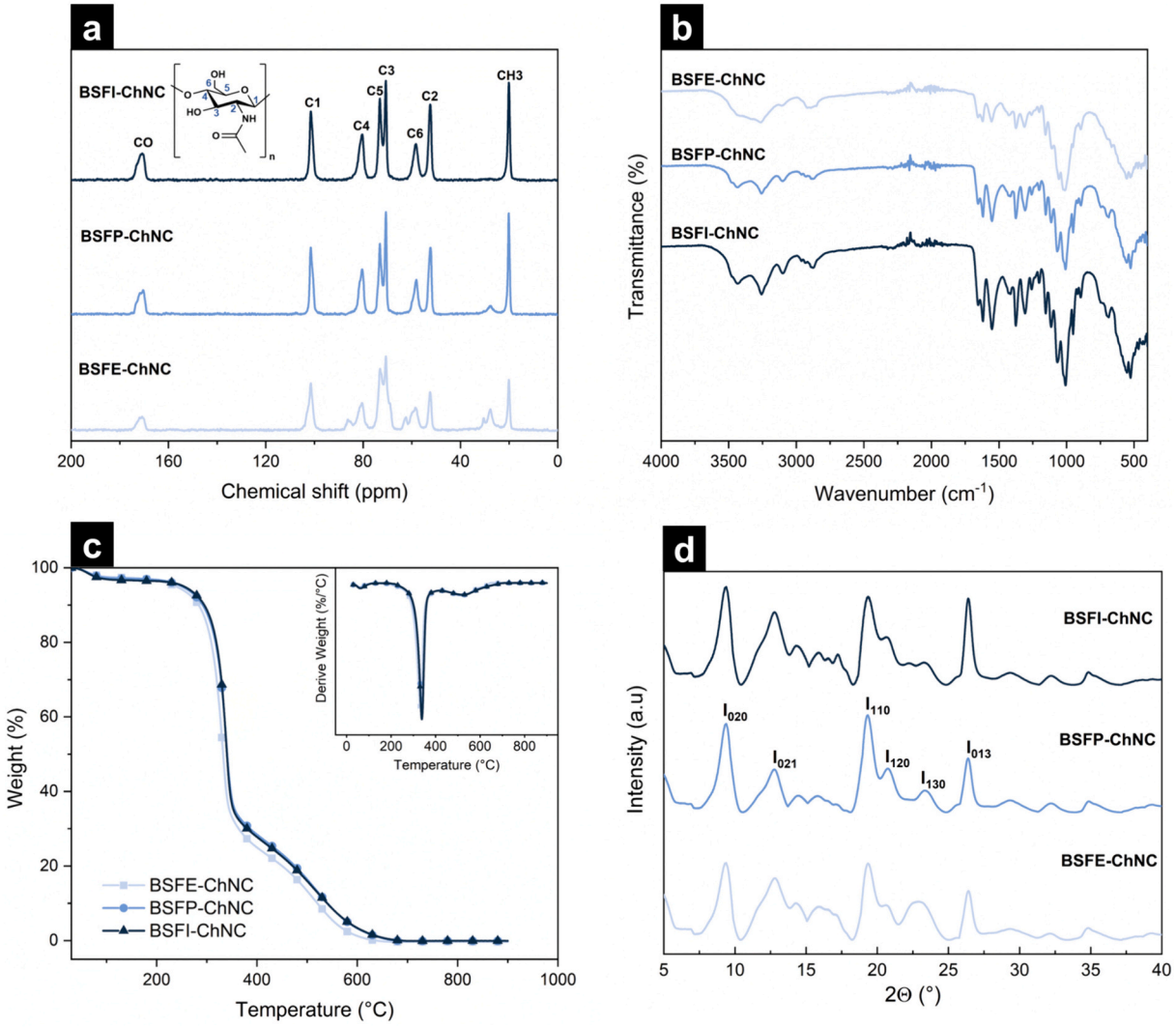

Fig. 3. ^{13}C NMR spectra (a), FTIR spectra (b), TGA and DTG profile under air atmosphere (c), and XRD diffractograms (d) of the chitin nanocrystals (ChNC) produced from BSF dead imago (BSFI-ChNC), BSF larval exuviae (BSFE-ChNC), and BSF puparium (BSFP-ChNC).

Recent research has reported an average height of 11 nm for chitin nanofibers obtained from BSF chitin larvae (Pasquier et al., 2021). The present data collected by AFM shows some aggregation of nanocrystals, in particular for the BSFP-ChNC sample which presents a high standard deviation. Consequently, although the data obtained gives a certain trend in the size of the nano-objects, a smaller average height for the chitin nanocrystals isolated in this study could be hypothesized, especially for BSFE-ChNC and BSFP-ChNC.

3.3.3. *Colloidal behaviour of the BSF-ChNCs*

The colloidal behaviour of the chitin nanocrystal suspensions was assessed by measuring their zeta potential at different pH (Table 3). Zeta potential gives insights into the charged groups at the surface of the considered nanoparticles, being a great tool to characterize their colloidal stability. In the case of chitin, charged groups can arise whether from positively charged ammonium ions ($-NH_3^+$), being more present for partially deacetylated ChNCs, or carboxylate anions ($-COO^-$) depending on the pH conditions. Herein, as illustrated in Fig. 5, for all samples a positive zeta potential was recorded at acidic pH, with close values for BSFI-ChNC and BSFP-ChNC, which then decreased gradually to negative zeta potential values comprised between −30 and − 40 mV at basic pH. For the BSFE-ChNC sample, a rather low zeta potential even at acidic pH could be associated with the presumed cellulose content, knowing that cellulose typically exhibits a negatively charged surface on a wide pH range. The overall following profiles were comparable to BSF ChNFs reported by Pasquier et al., even though BSF ChNCs isolated in the current study shifted to negative zeta potential at lower pH than BSF ChNFs, resulting in higher negative values at neutral pH for nanocrystals (Pasquier et al., 2021). This could be due to the higher acetylation degree, indicating a limited presence of ammonium ions, thus, resulting in a reduced stabilization of ChNCs. Previous studies have reported that flocculation of nanoparticles is often encountered for zeta potential values between −15 and 15 mV, and usually stable for values above 25 mV highlighting that a high zeta potential is necessary to display enhanced colloidal stability (Naduparambath et al., 2018); (Morais et al., 2013); (Melikoğlu et al., 2019). For instance, Ngasotter et al. reported stable ChNCs obtained from shrimp shells with a zeta potential value of 51.1 mV (Ngasotter et al., 2023). This could be linked to the aggregation behaviour of BSF ChNCs isolated in the current study which can be correlated to the *Z*-average diameters recorded for the nanocrystal's suspensions (see Supplementary Fig. S8).

When measuring the size parameters of nanocrystals in DLS, a critical approach should be adopted because those nano-objects are not spherical and usually display a high aspect ratio (Tarrés et al., 2022). However, Z-average diameters of BSF ChNCs ranged from 250 nm to 740 nm depending on the sample and the pH conditions (see Fig. S8),

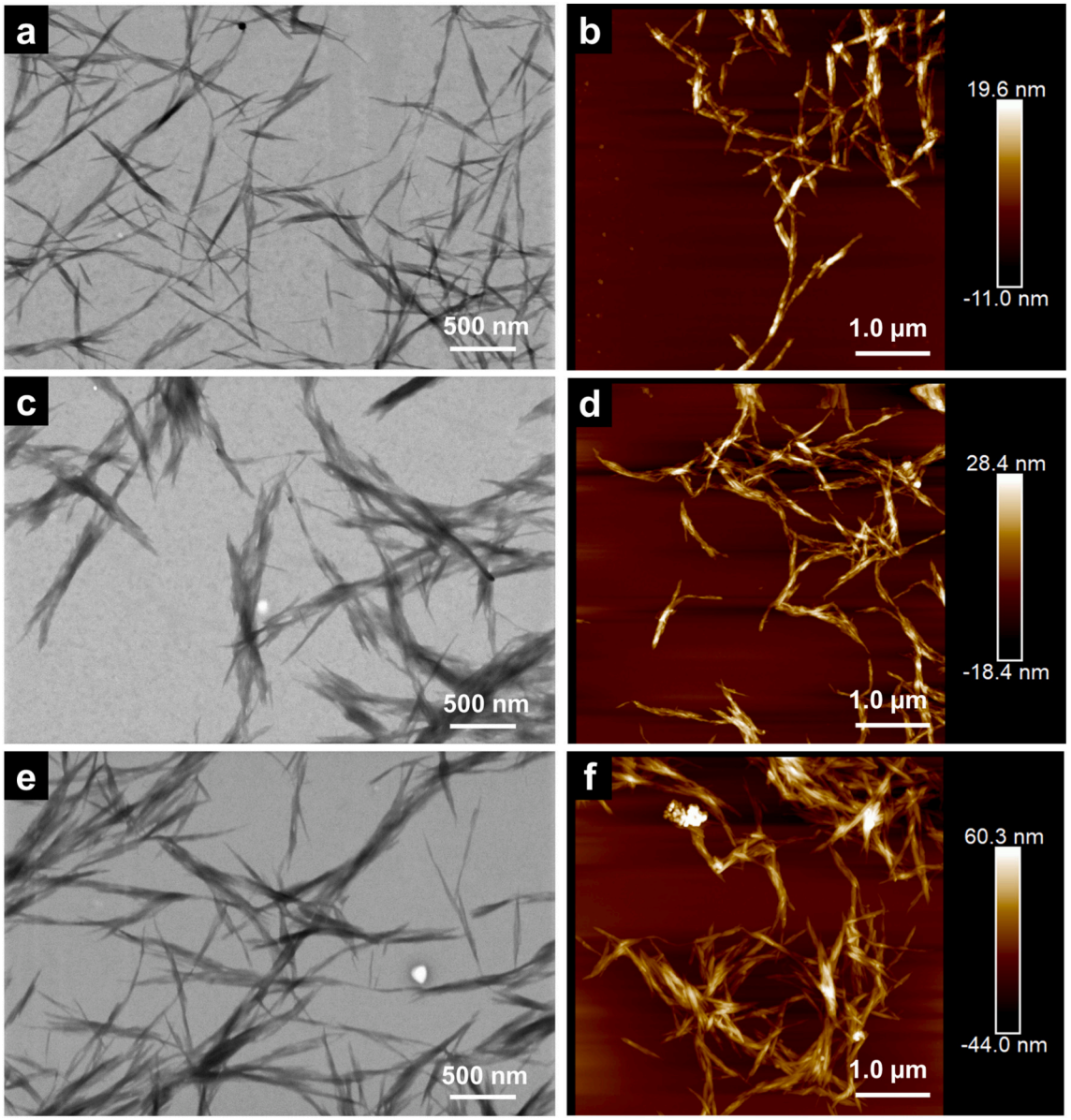

Fig. 4. STEM in SEM in BF mode and AFM images in peak force mode of chitin nanocrystals (ChNCs) isolated from BSF dead imago (BSFI-ChNC) (a,b), BSF larval exuviae (BSFE-ChNC) (c,d), and BSF puparium (BSFP-ChNC) (e,f) (STEM: a,c,e; AFM: b,d,f).

Table 3
Chitin nanocrystal height measured from AFM images and zeta potential values of diluted ChNCs suspensions at different pH.

Sample name	Minimum ChNC height (nm)	Maximum ChNC height (nm)	Average ChNC height (nm)	Zeta potential at pH 2 (mV)	Zeta potential at pH 7 (mV)	Zeta potential at pH 12 (mV)
BSFE-ChNC	11.72	48.49	21.00 ± 6.90	3.12 ± 0.72	−17.17 ± 0.85	−36.83 ± 1.46
BSFP-ChNC	16.00	106.98	27.23 ± 17.28	12.80 ± 1.31	−20.90 ± 0.56	−29.80 ± 1.38
BSFI-ChNC	6.59	31.25	13.35 ± 5.69	10.90 ± 1.06	−21.00 ± 2.87	−39.20 ± 0.49

Average height is presented as mean ± standard deviation ($n = 50$) and zeta potential value as mean ± standard deviation ($n = 3$).

being aggregated in the case of high Z-average value, which was consistent with the literature (Ngasotter et al., 2023); (Jin et al., 2022). These results suggest that the slight decrease in Z-average diameter observed at pH of around 8 to 10 for all chitin nanocrystals seems to be correlated to the higher zeta potential in absolute value at this pH range. Therefore, in the current work, BSF ChNCs are thought to be essentially stabilized by the carboxylate anions and hydrophobic repulsion of the acetyl groups. Thus, an enhanced colloidal stability would be reached at slightly basic to basic pH ($8 \geq$ pH ≤ 10). This represents a key aspect in the use of the BSF ChNCs as reinforcing agent in nanocomposite for active packaging, aerogels for thermal insulation, or as stabilization agent in Pickering emulsion for food or bio-elastomers development (Fernández-Marín et al., 2020); (Yan et al., 2020); (Barkhordari & Fathi, 2018); (Wang et al., 2017).

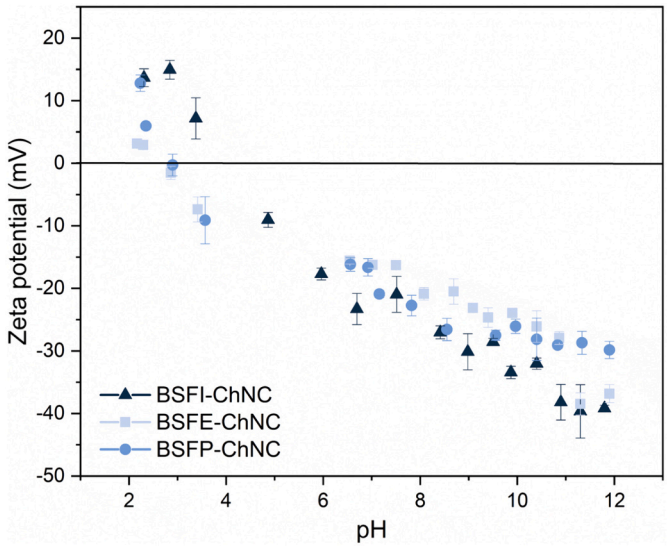

Fig. 5. Zeta potential values of the ChNCs suspensions in function of the pH obtained from BSF dead imago (BSFI-ChNC), BSF larval exuviae (BSFE-ChNC) and BSF puparium (BSFP-ChNC) (data are presented as mean ± standard deviation with n = 3).

4. Conclusion

In this study, the valorisation of three types of resources produced as rearing waste during the life cycle of *H. illucens* (the larval exuviae – larval moult, the puparium – pupal shell left after fly emergence, and the dead imago – dead fly) were considered as potential alternative sources of chitin and chitin nanocrystals. The extracted chitins and chitin nanocrystals were characterized regarding their yield, physico-chemical, thermal and morphological properties.

Chitins derived from dead adult (BSFI-Ch) and puparium (BSFP-Ch) were comparable to the one obtained from shrimp commercial chitin, exhibiting a high DA (97–100 %), with thermal and chemical features characteristics of the α-chitin polymorph, displaying a maximal degradation temperature between 370 and 395 °C under inert atmosphere. Some residual proteins were found in extracts from moults (i.e., puparium and larval exuviae) while BSFI-Ch was confirmed to display a higher degree of purity. Other impurities were detected for the larval exuviae sample, possibly linked to a cellulosic content introduced during biomass harvesting from the breeding crate. Therefore, among the considered initial resources, puparium stands-out in the scope of chitin production, with a high extraction yield of around 20 %.

Chitin nanocrystals were subsequently isolated from chitin extracted from BSF by-products, revealing similar physico-chemical properties than their chitin analogues, although showing an apparent increase in purity according to TGA profiles and FTIR spectra. STEM in SEM and AFM investigations highlighted a rod-like morphology for all the chitin nanocrystals isolated from BSF by-product. Nanocrystals average height of around 13 to 27 nm was estimated from AFM analysis depending on the sample. The analysis of the zeta potential of the ChNC suspensions at different pH, showed a better colloidal stability at slight basic to basic pH with zeta potential values close to −30 mV, implying a less aggregate state and smaller nanoparticle size. Those data are of crucial importance, when considering the suitable condition to process the obtained nanocrystals and optimize their use in material applications.

The present work, provide fundamental insights to understand the composition, intrinsic physico-chemical and morphological properties of the chitins and chitin nanocrystals obtained from each BSF by-product. Taking in account their properties, that are very similar to those from commercial chitin from crustacea, these samples have potential promising applications in nanocomposites or Pickering emulsions for food technology, cosmetics or packaging.

From an industrial point of view, thousands of tonnes of by-products are generated each year in this sector, which represents non-seasonal available biomass to be upgraded into high value-added products such as chitin and its derivatives. Other interesting reflexions would be the production of chitin from the whole by-products or similar resources (i.e., larval exuviae and puparium), gathered in a unique process adapted to extract BSF chitin with the highest purity, and also to try to valorise the other compounds of these by-products like the lipids and proteins using a biorefinery approach. Also, for future studies, it will be crucial to focus on translation towards more resilient extraction processes within the framework of green chemistry, adapting new type of solvent to process this insect biomass, using fundamental tools to assess the generated impact on the environment (LCA, GAPI metrics) as well as an evaluation of the economic viability of the created process.

Knowing that insect meals have been subject to new regulations in the EU and that the physicochemical characteristics of insect chitins are close to those of crustacean chitins, similar regulatory aspects and potential applications are expected for BSF chitin-rich by-product derivatives.

Funding

This work was funded by the company Agronutris with support from the French Ministry of Higher Education, Research and Innovation in the frame of a CIFRE (grant number #2022/0421) PhD grant attributed by the French National Association for Research and Technology. The company did not interfere with the conclusions of the study. It was also carried under the framework of E2S UPPA Partnership Chair MANTA (Marine Materials) funded by the 'Investissements d'Avenir' French program managed by ANR, grant number #ANR-16-IDEX-0002.

CRediT authorship contribution statement

Alexis Falgayrac: Writing – original draft, Validation, Methodology, Data curation, Conceptualization. **Virginie Pellerin:** Methodology, Data curation. **Cécile Terrol:** Validation, Supervision. **Susana C.M. Fernandes:** Writing – review & editing, Validation, Supervision, Project administration, Formal analysis, Conceptualization.

Declaration of competing interest

The authors declare that they have no known competing financial interests or personal relationships that could have appeared to influence the work reported in this paper.

Susana Fernandes reports financial support was provided by French National Association for Research and Technology. Susana Fernandes reports financial support was provided by French National Association for Research. If there are other authors, they declare that they have no known competing financial interests or personal relationships that could have appeared to influence the work reported in this paper.

Data availability

No data was used for the research described in the article.

Acknowledgement

The authors would like to thank Agronutris and the French Ministry of Higher Education, Research and Innovation for their funding. The authors also acknowledge Dr. Natalia Castejón and Dr. Sheila Olza for their involvement in the first extraction trials.

Appendix A. Supplementary data

Supplementary data to this article can be found online at https://doi.

org/10.1016/j.carbpol.2024.122545.

References

Andersen, S. O. (2010). Insect cuticular sclerotization: A review. *Insect Biochemistry and Molecular Biology, 40*(3), 166–178. https://doi.org/10.1016/j.ibmb.2009.10.007

Arnold, N. D., Brück, W. M., Garbe, D., & Brück, T. B. (2020). Enzymatic modification of native chitin and conversion to specialty chemical products. *Marine Drugs, 18*(2), 2. https://doi.org/10.3390/md18020093

Arrese, E. L., & Soulages, J. L. (2010). Insect fat body: Energy, metabolism, and regulation. *Annual Review of Entomology, 55*, 207–225. https://doi.org/10.1146/annurev-ento-112408-085356

Bai, L., Liu, L., Esquivel, M., Tardy, B. L., Huan, S., Niu, X., … Rojas, O. J. (2022). Nanochitin: Chemistry, structure, assembly, and applications. *Chemical Reviews, acs.chemrev.2c00125*. https://doi.org/10.1021/acs.chemrev.2c00125

Barkhordari, M. R., & Fathi, M. (2018). Production and characterization of chitin nanocrystals from prawn shell and their application for stabilization of Pickering emulsions. *Food Hydrocolloids, 82*, 338–345. https://doi.org/10.1016/j.foodhyd.2018.04.030

Bhavsar, P. S., Dalla Fontana, G., & Zoccola, M. (2021). Sustainable superheated water hydrolysis of black soldier Fly Exuviae for chitin extraction and use of the obtained chitosan in the textile field. *ACS Omega, 6*(13), 8884–8893. https://doi.org/10.1021/acsomega.0c06040

Brigode, C., Hobbi, P., Jafari, H., Verwilghen, F., Baeten, E., & Shavandi, A. (2020). Isolation and physicochemical properties of chitin polymer from insect farm side stream as a new source of renewable biopolymer. *Journal of Cleaner Production, 275*, Article 122924. https://doi.org/10.1016/j.jclepro.2020.122924

Chavez, M. (2021). The sustainability of industrial insect mass rearing for food and feed production: Zero waste goals through by-product utilization. *Current Opinion in Insect Science, 48*, 44–49. https://doi.org/10.1016/j.cois.2021.09.003

Elkadaoui, S., Azzi, M., Desbrieres, J., Zim, J., El Hachimi, Y., & Tolaimate, A. (2024). Valorization of *Hermetia illucens* breeding rejects by chitins and chitosans production. Influence of processes and life cycle on their physicochemical characteristics. *International Journal of Biological Macromolecules, 131314*. https://doi.org/10.1016/j.ijbiomac.2024.131314

Feng, H., Wang, Z., Sajab, M. S., Abdul, P. M., & Ding, G. (2023). A novel chitinous nanoparticles prepared and characterized with black soldier fly (*Hermetia illucens L.*) using steam flash explosion treatment. *International Journal of Biological Macromolecules, 230*, Article 123210. https://doi.org/10.1016/j.ijbiomac.2023.123210

Fernández-Marín, R., Fernandes, S. C. M., Sánchez, M.Á. A., & Labidi, J. (2022). Halochromic and antioxidant capacity of smart films of chitosan/chitin nanocrystals with curcuma oil and anthocyanins. *Food Hydrocolloids, 123*, Article 107119. https://doi.org/10.1016/j.foodhyd.2021.107119

Fernández-Marín, R., Labidi, J., Andrés, M.Á., & Fernandes, S. C. M. (2020). Using α-chitin nanocrystals to improve the final properties of poly (vinyl alcohol) films with Origanum vulgare essential oil. *Polymer Degradation and Stability, 179*, Article 109227. https://doi.org/10.1016/j.polymdegradstab. 2020.109227

Fernández-Marín, R., Mujtaba, M., Cansaran-Duman, D., Ben Salha, G., Andrés Sánchez, M.Á., Labidi, J., & Fernandes, S. C. M. (2021). Effect of Deterpenated Origanum majorana L. *Essential Oil on the Physicochemical and Biological Properties of Chitosan/β-Chitin Nanofibers Nanocomposite Films. Polymers, 13*(9), 9. https://doi.org/10.3390/polym13091507

Gopalan Nair, K., Dufresne, A., Gandini, A., & Belgacem, M. N. (2003). Crab Shell chitin whiskers reinforced natural rubber nanocomposites. 3. Effect of chemical modification of chitin whiskers. *Biomacromolecules, 4*(6), 1835–1842. https://doi.org/10.1021/bm030058g

Hahn, T., Tafi, E., Paul, A., Salvia, R., Falabella, P., & Zibek, S. (2020). Current state of chitin purification and chitosan production from insects. *Journal of Chemical Technology & Biotechnology, 95*(11), 2775–2795. https://doi.org/10.1002/jctb.6533

Hahn, T., Tafi, E., von Seggern, N., Falabella, P., Salvia, R., Thomä, J., … Zibek, S. (2021). *Purification of chitin from pupal Exuviae of the black soldier Fly*. Waste and Biomass Valorization: Scopus. https://doi.org/10.1007/s12649-021-01645-1

Jia, Z., Deng, Z., & Li, L. (2022). Biomineralized materials as model Systems for Structural Composites: 3D architecture. *Advanced Materials, 34*(20), 2106259. https://doi.org/10.1002/adma.202106259

Jiménez-Saelices, C., Trongsatitkul, T., Lourdin, D., & Capron, I. (2020). Chitin Pickering emulsion for oil inclusion in composite films. *Carbohydrate Polymers, 242*, Article 116366. https://doi.org/10.1016/j.carbpol.2020.116366

Jin, T., Liu, T., Hajiali, F., Santos, M., Liu, Y., Kurdyla, D., … Moores, A. (2022). High-humidity shaker aging to access chitin and cellulose nanocrystals**. *Angewandte Chemie International Edition, 61*(42), Article e202207206. https://doi.org/10.1002/anie.202207206

Kamal, M., Adly, E., Alharbi, S. A., Khaled, A. S., Rady, M. H., & Ibrahim, N. A. (2020). Exploring simplified methods for insect chitin extraction and application as a potential alternative bioethanol resource. *Insects, 11*(11), 11. https://doi.org/10.3390/insects11110788

Kasaai, M. R. (2010). Determination of the degree of N-acetylation for chitin and chitosan by various NMR spectroscopy techniques: A review. *Carbohydrate Polymers, 79*(4), 801–810. https://doi.org/10.1016/j.carbpol.2009.10.051

Kaya, M., & Baran, T. (2015). Description of a new surface morphology for chitin extracted from wings of cockroach (Periplaneta americana). *International Journal of Biological Macromolecules, 75*, 7–12. https://doi.org/10.1016/j.ijbiomac.2015.01.015

Kaya, M., Erdogan, S., Mol, A., & Baran, T. (2015). Comparison of chitin structures isolated from seven Orthoptera species. *International Journal of Biological Macromolecules, 72*, 797–805. https://doi.org/10.1016/j.ijbiomac.2014.09.034

Kaya, M., Mujtaba, M., Ehrlich, H., Salaberria, A. M., Baran, T., Amemiya, C. T., … Labidi, J. (2017). On chemistry of γ-chitin. *Carbohydrate Polymers, 176*, 177–186. https://doi.org/10.1016/j.carbpol.2017.08.076

Khatami, N., Guerrero, P., Martín, P., Quintela, E., Ramos, V., Saa, L., … Abarrategi, A. (2024). Valorization of biological waste from insect-based food industry: Assessment of chitin and chitosan potential. *Carbohydrate Polymers, 324*, Article 121529. https://doi.org/10.1016/j.carbpol.2023.121529

Kishida, K., Mizuta, T., Izawa, H., & Ifuku, S. (2022). Preparation of Nanochitin from Crickets and Comparison with That from Crab Shells. *Journal of Composites Science*, *6*(10). Scopus. doi:https://doi.org/10.3390/jcs6100280.

Kramer, K. J., Hopkins, T. L., & Schaefer, J. (1995). Applications of solids NMR to the analysis of insect sclerotized structures. *Insect Biochemistry and Molecular Biology, 25*(10), 1067–1080. https://doi.org/10.1016/0965-1748(95)00053-4

Le, T. M., Tran, C. L., Nguyen, T. X., Duong, Y. H. P., Le, P. K., & Tran, V. T. (2023). Green preparation of chitin and Nanochitin from black soldier Fly for production of biodegradable packaging material. *Journal of Polymers and the Environment.*. https://doi.org/10.1007/s10924-023-02793-2

Lee, Y. H., Kim, S. C., Nam, K. D., Kim, T. H., Jung, B. O., Park, Y.-I., … Park, J. K. (2022). Chitosan isolated from black soldier flies Hermetia illucens: Structure and enzymatic hydrolysis. *Process Biochemistry, 118*, 171–181. https://doi.org/10.1016/j.procbio.2022.04.020

Lv, J., Lv, X., Ma, M., Oh, D.-H., Jiang, Z., & Fu, X. (2023). Chitin and chitin-based biomaterials: A review of advances in processing and food applications. *Carbohydrate Polymers, 299*, Article 120142. https://doi.org/10.1016/j.carbpol.2022.120142

Mannucci, A., Panariello, L., Abenaim, L., Coltelli, M. B., Ranieri, A., Conti, B., … Castagna, A. (2024). From food waste to functional biopolymers: Characterization of chitin and chitosan produced from Prepupae of black soldier Fly reared with different food waste-based diets. *Foods, 13*(2), 2. https://doi.org/10.3390/foods13020278

McReynolds, C., Adrien, A., Petitpas, A., Rubatat, L., & Fernandes, S. C. M. (2022). Double valorization for a discard—α-chitin and calcium lactate production from the crab Polybius henslowii using a deep eutectic solvent approach. *Marine Drugs, 20*(11), 11. https://doi.org/10.3390/md20110717

Melikoğlu, A. Y., Bilek, S. E., & Cesur, S. (2019). Optimum alkaline treatment parameters for the extraction of cellulose and production of cellulose nanocrystals from apple pomace. *Carbohydrate Polymers, 215*, 330–337. https://doi.org/10.1016/j.carbpol.2019.03.103

Miller, E. L., Bimbo, A. P., Barlow, S. M., SHeridan, B., Burks, L. B. W., & Collaborators. (2007). Repeatability and reproducibility of determination of the nitrogen content of fishmeal by the combustion (dumas) method and comparison with the Kjeldahl method: Interlaboratory study. *Journal of AOAC International, 90*(1), 6–20. https://doi.org/10.1093/jaoac/90.1.6

Morais, J. P. S., Rosa, M.d. F., de Souza Filho, M.d.s. M., Nascimento, L. D., do Nascimento, D. M., & Cassales, A. R. (2013). Extraction and characterization of nanocellulose structures from raw cotton linter. *Carbohydrate Polymers, 91*(1), 229–235. https://doi.org/10.1016/j.carbpol.2012.08.010

Muthukrishnan, S., Arakane, Y., Noh, M. Y., Mun, S., Merzendorfer, H., Boehringer, C., … Liu, L. (2022). Chitin in insect cuticle. In *, Vol. 62. Advances in insect physiology* (pp. 1–110). Elsevier. https://doi.org/10.1016/bs.aiip.2022.03.001.

Naduparambath, S., T.v., J., V., S., M.p., S., Balan, A. K., & E., P. (2018). Isolation and characterisation of cellulose nanocrystals from sago seed shells. *Carbohydrate Polymers, 180*, 13–20. https://doi.org/10.1016/j.carbpol.2017.09.088

Narkevicius, A., Steiner, L. M., Parker, R. M., Ogawa, Y., Frka-Petesic, B., & Vignolini, S. (2019). Controlling the self-assembly behavior of aqueous chitin nanocrystal suspensions. *Biomacromolecules, 20*(7), 2830–2838. https://doi.org/10.1021/acs.biomac.9b00589

Ngasotter, S., Xavier, K. A. M., Porayil, L., Balange, A., Nayak, B. B., Eapen, S., … Ninan, G. (2023). Optimized high-yield synthesis of chitin nanocrystals from shrimp shell chitin by steam explosion. *Carbohydrate Polymers, 316*, Article 121040. https://doi.org/10.1016/j.carbpol.2023.121040

Nurfikari, A., & de Boer, W. (2021). Chitin determination in residual streams derived from insect production by LC-ECD and LC-MS/MS methods. *Frontiers in Sustainable Food Systems, 5*. https://www.frontiersin.org/article/10.3389/fsufs.2021.795694.

OECD. (2019). OECD-FAO Agricultural Outlook 2019–2028. Organisation for Economic Co-operation and Development https://www.oecd-ilibrary.org/agriculture-and-food/oecd-fao-agricultural-outlook-2019-2028_agr_outlook-2019-en.

Ojha, S., Bußler, S., & Schlüter, O. K. (2020). Food waste valorisation and circular economy concepts in insect production and processing. *Waste Management, 118*, 600–609. https://doi.org/10.1016/j.wasman.2020.09.010

Olza, S., Salaberria, A. M., Alonso-Varona, A., Samanta, A., & Fernandes, S. C. M. (2023). The role of nanochitin in biologically-active matrices for tissue engineering-where do we stand? *Journal of Materials Chemistry B.*. https://doi.org/10.1039/D3TB00583F

Pasquier, E., Beaumont, M., Mattos, B. D., Otoni, C. G., Winter, A., Rosenau, T., … Bras, J. (2021). Upcycling byproducts from insect (Fly larvae and mealworm) farming into chitin nanofibers and films. *ACS Sustainable Chemistry & Engineering, 9*(40), 13618–13629. https://doi.org/10.1021/acssuschemeng.1c05035

Paulino, A. T., Simionato, J. I., Garcia, J. C., & Nozaki, J. (2006). Characterization of chitosan and chitin produced from silkworm crysalides. *Carbohydrate Polymers, 64*(1), 98–103. https://doi.org/10.1016/j.carbpol.2005.10.032

Peter, M. G., Grün, L., & Förster, H. (1984). CP/MAS-13C-NMR spectra of sclerotized insect cuticle and of chitin. *Angewandte Chemie International Edition in English, 23*(8), 638–639. https://doi.org/10.1002/anie.198406381

Purkayastha, D., & Sarkar, S. (2020). Physicochemical structure analysis of chitin extracted from Pupa Exuviae and dead imago of wild black soldier Fly (Hermetia illucens). *Journal of Polymers and the Environment, 28*(2), 445–457. https://doi.org/10.1007/s10924-019-01620-x

Rampure, S. M., Velayudhannair, K., & Marimuthu, N. (2023). Characteristics of chitin extracted from different growth phases of black soldier fly, Hermetia illucens, fed with different organic wastes. *International Journal of Tropical Insect Science, 43*(3), 979–987. https://doi.org/10.1007/s42690-023-00997-6

Rebora, M., Salerno, G., Piersanti, S., Saitta, V., Morelli Venturi, D., Li, C., & Gorb, S. (2023). The armoured cuticle of the black soldier fly Hermetia illucens. *Scientific Reports, 13*(1), 1. https://doi.org/10.1038/s41598-023-49549-5

Salaberria, A. M., Diaz, R., Andrés, M. A., Fernandes, S. C. M., & Labidi, J. (2017). The antifungal activity of functionalized chitin nanocrystals in poly(lactic acid) films. *Materials, 10*, 546. https://doi.org/10.3390/ma10050546

Salaberria, A. M., Labidi, J., & Fernandes, S. C. M. (2014). Chitin nanocrystals and nanofibers as nano-sized fillers into thermoplastic starch-based biocomposites processed by melt-mixing. *Chemical Engineering Journal, 256*, 356–364. https://doi.org/10.1016/j.cej.2014.07.009

Salaberria, A. M., Labidi, J., & Fernandes, S. C. M. (2015). Different routes to turn chitin into stunning nano-objects. *European Polymer Journal, 68*, 503–515. https://doi.org/10.1016/j.eurpolymj.2015.03.005

Sharp, R. G. (2013). A review of the applications of chitin and its derivatives in agriculture to modify plant-microbial interactions and improve crop yields. *Agronomy, 3*(4), 4. https://doi.org/10.3390/agronomy3040757

Soetemans, L., Uyttebroek, M., & Bastiaens, L. (2020). Characteristics of chitin extracted from black soldier fly in different life stages. *International Journal of Biological Macromolecules, 165*, 3206–3214. https://doi.org/10.1016/j.ijbiomac.2020.11.041

Springmann, M., Clark, M., Mason-D'Croz, D., Wiebe, K., Bodirsky, B. L., Lassaletta, L., … Willett, W. (2018). Options for keeping the food system within environmental limits. *Nature, 562*(7728), 519–525. https://doi.org/10.1038/s41586-018-0594-0

Tamura, H., Furuike, T., Nair, S. V., & Jayakumar, R. (2011). Biomedical applications of chitin hydrogel membranes and scaffolds. *Carbohydrate Polymers, 84*(2), 820–824. https://doi.org/10.1016/j.carbpol.2010.06.001

Tarrés, Q., Aguado, R., Zoppe, J. O., Mutjé, P., Fiol, N., & Delgado-Aguilar, M. (2022). Dynamic light scattering plus scanning Electron microscopy: Usefulness and limitations of a simplified estimation of Nanocellulose dimensions. *Nanomaterials, 12*(23), 23. https://doi.org/10.3390/nano12234288

Triunfo, M., Tafi, E., Guarnieri, A., Salvia, R., Scieuzo, C., Hahn, T., … Falabella, P. (2022). Characterization of chitin and chitosan derived from Hermetia illucens, a further step in a circular economy process. *Scientific Reports, 12*(1), 6613. https://doi.org/10.1038/s41598-022-10423-5

van Huis, A. (2013). *Edible insects: Future prospects for food and feed security* (Food and Agriculture Organization of the United Nations).

Wang, H., Rehman, K.u., Feng, W., Yang, D., Rehman, R.u., Cai, M., … Zheng, L. (2020). Physicochemical structure of chitin in the developing stages of black soldier fly. *International Journal of Biological Macromolecules, 149*, 901–907. https://doi.org/10.1016/j.ijbiomac.2020.01.293

Wang, X., Liang, K., Tian, Y., & Ji, Y. (2017). A facile and green emulsion casting method to prepare chitin nanocrystal reinforced citrate-based bioelastomer. *Carbohydrate Polymers, 157*, 620–628. https://doi.org/10.1016/j.carbpol.2016.10.034

Xiong, A., Ruan, L., Ye, K., Huang, Z., & Yu, C. (2023). Extraction of chitin from black soldier Fly (Hermetia illucens) and its Puparium by using biological treatment. *Life, 13*(7), 7. https://doi.org/10.3390/life13071424

Yan, Y., Ge, F., Qin, Y., Ruan, M., Guo, Z., He, C., & Wang, Z. (2020). Ultralight and robust aerogels based on nanochitin towards water-resistant thermal insulators. *Carbohydrate Polymers, 248*, Article 116755. https://doi.org/10.1016/j.carbpol.2020.116755

Złotko, K., Waśko, A., Kamiński, D. M., Budziak-Wieczorek, I., Bulak, P., & Bieganowski, A. (2021). Isolation of chitin from black soldier Fly (Hermetia illucens) and its usage to metal sorption. *Polymers, 13*(5), 5. https://doi.org/10.3390/polym13050818

Zozo, B., Wicht, M. M., Mshayisa, V. V., & van Wyk, J. (2022). The nutritional quality and structural analysis of black soldier Fly larvae flour before and after defatting. *Insects, 13*(2), 2. https://doi.org/10.3390/insects13020168

Zubillaga, V., Alonso-Varona, A., Fernandes, S. C. M., Salaberria, A. M., & Palomares, T. (2020). Adipose-derived mesenchymal Stem cell Chondrospheroids cultured in hypoxia and a 3D porous chitosan/chitin nanocrystal scaffold as a platform for cartilage tissue engineering. *International Journal of Molecular Sciences, 21*(3), 3. https://doi.org/10.3390/ijms21031004

Zubillaga, V., Salaberria, A. M., Palomares, T., Alonso-Varona, A., Kootala, S., Labidi, J., & Fernandes, S. C. M. (2018). Chitin Nanoforms provide mechanical and topological cues to support growth of human adipose Stem cells in chitosan matrices. *Biomacromolecules, 19*(7), 3000–3012. https://doi.org/10.1021/acs.biomac.8b00570